

Journal of
**Micro/Nanolithography,
MEMS, and MOEMS**

SPIDigitalLibrary.org/jm3

**Improved micro-optoelectromechanical
systems deformable mirror for *in vivo*
optical microscopy**

Mohammad J. Moghimi
Chris R. Wilson
David L. Dickensheets

Improved micro-optoelectromechanical systems deformable mirror for *in vivo* optical microscopy

Mohammad J. Moghimi
Montana State University
Department of Electrical and Computer
Engineering
511 Cobleigh Hall
Bozeman, Montana 59717

Chris R. Wilson
Bridger Photonics, Inc.
2310 University Way, Building 4-4
Bozeman, Montana 59717

David L. Dickensheets
Montana State University
Department of Electrical and Computer
Engineering
530 Cobleigh Hall
Bozeman, Montana 59717
E-mail: davidd@ee.montana.edu

Abstract. Micro-optoelectromechanical systems (MOEMS) deformable mirrors are being developed for focus control in miniature optical systems including endoscopic microscopes and small form-factor camera lenses. A new process is described to create membrane mirrors made from the photoset polymer SU-8. The SU-8 also serves as the adhesive layer for wafer bonding, resulting in a simple, low cost fabrication process. The process details and the optical properties of the resulting focus control mirrors, which have a diameter of 2 mm, a stroke in excess of 8 μm and very low residual aberration, are described. Multiple actuation electrodes allow active control of more than 1.4 μm peak-to-peak of wavefront spherical aberration. The MOEMS mirror is demonstrated in a confocal microscope in which it provides focus control during capture of *in vivo* images. © 2012 Society of Photo-Optical Instrumentation Engineers (SPIE). [DOI: [10.1117/1.JMM.11.4.043006](https://doi.org/10.1117/1.JMM.11.4.043006)]

Subject terms: micro-optoelectromechanical systems deformable mirror; focus control; SU-8; wafer bonding.

Paper 12051P received Jun. 11, 2012; revised manuscript received Aug. 25, 2012; accepted for publication Sep. 17, 2012; published online Oct. 12, 2012.

1 Introduction

Agile optical focus control is essential for vital microscopy to provide images at variable depth within intact tissue. *In vivo* optical microscopy for diagnosis of diseases such as cancer is a primary motivation for the development of new focus control methods that are fast and can be miniaturized for handheld or endoscopic instruments. Additionally, miniaturized means for dynamic focus control may be useful for cell phone cameras, three-dimensional optical switches and pico-projectors. The conventional method of focus control using lens translation with motors and cams leads to increased mechanical complexity, high power consumption and is relatively slow.

Micro-optoelectromechanical systems (MOEMS) variable-power optics is a promising alternative to lens translation for focus control. One example is electro-wetting transmissive variable focus lenses that can adjust focal length by varying the curvature of a liquid interface. This type of lens is able to achieve large focusing power, but potential problems include liquid evaporation and shock stability^{1–4} and limited adaptive control of the detailed shape of the optical surface. Another approach is the MOEMS liquid pneumatic lens.^{5–13} In this type of element, pumping a liquid in and out of an optically transparent cavity with an elastic membrane changes the curvature in order to control focus. The liquid-filled lens requires a mechanical pumping system and may exhibit vibration sensitivity.³ Liquid lenses (both electrowetting and pneumatic) also require careful thermal engineering and may pose problems for low temperature operation. In contrast, electrostatic membrane mirrors are simple, achromatic, low power and relatively fast, and use of multiple actuation electrodes allows precise control of

mirror shape to control both focal length and spherical aberration.^{14,15}

The optical and mechanical properties of the membrane are important to the performance of this device as a deformable mirror. Stress in the membrane material influences the maximum membrane displacement and focus range, and stress nonuniformity leads to aberration due to compromised surface flatness. Several materials have been demonstrated for focus control mirrors. Early mirrors using silicon nitride membranes^{16,17} exhibited good stress uniformity and low aberrations, but suffered from high intrinsic stress that limited overall displacement. More recent work with polymers including SU-8,^{14,15} Cytop¹⁸ and Polyimide¹⁹ achieve larger deflection due to lower film stress. Except for the surface micromachined devices,²⁰ these latter techniques employ bonding of a spin-cast membrane wafer to an electrode-bearing substrate wafer with some spacer material in between. The bonding and assembly steps are critical to maintaining uniform stress in the resulting free-standing membranes. Previously we reported SU-8 membrane mirrors constructed using a die bonding technique, in which a silicon die with a wet-etch released membrane was aligned and glued to a die that supported a spacer and the electrostatic actuation electrodes.¹⁵ Errors during alignment and bonding led to nonuniform initial stress in the suspended membrane, residual aberrations and poor device repeatability. Other mirrors^{14,19} also show residual aberration when not actuated, relying on active flattening using an electrode array with a large number of actuators. By comparison, our focus control mirrors have circularly symmetric ring electrodes and must have excellent initial flatness to achieve the targeted control of focus and (circularly symmetric) spherical aberration without introducing unwanted residual aberrations.

In this paper, we describe a new fabrication process using wafer bonding and dry etching to achieve more uniform

in-plane stress to minimize residual aberration on the membrane mirror. The mirrors are made from metalized photoset polymer SU-8 which has excellent mechanical properties, including relatively low residual stress in the range of 14 to 30 MPa depending on process parameters²¹ to enable large electrostatic deflection. The SU-8 also serves as an adhesive layer for wafer bonding, resulting in a simple and low cost fabrication process. The membrane mirrors are released after the wafer bonding step using deep reactive-ion etching (DRIE) producing a flat, reflective and uniform surface. The surface quality and membrane displacement are measured using an optical interferometer and the results show that the new process improves the initial flatness and reduces the residual aberration of our SU-8 membrane mirrors. The focus range and active spherical aberration correction are also investigated for these deformable mirrors, and we demonstrate for the first time the use of this mirror for focus control in a scanning confocal microscope while imaging to a depth of up to 100 μm in live plant tissue, with a mirror-controlled range of focus of 42 μm using an objective lens with NA = 0.9.

2 Principle of Operation

An electrostatic MOEMS deformable mirror consists of a reflecting thin membrane suspended over actuating electrodes. The electrodes are patterned as three circular concentric rings. The electrodes and membrane are separated by a spacer layer. By applying a voltage between the membrane and any given electrode, an electrostatic force pulls the membrane toward the electrodes and the mirror can be deformed to the required shape. A curved reflector provides optical power, causing a reflected beam to come to a focus. As illustrated in Fig. 1(a), a greater deflection results in greater optical power and a shorter focal length.

In terms of the applied voltage $V(r)$, the electrostatic pressure on the membrane is

$$p(r) = \frac{\epsilon_0 V^2(r)}{2[g - s(r)]^2}, \quad (1)$$

where g is the air gap beneath the membrane, $s(r)$ is the membrane deflection toward the substrate, ϵ_0 is the

permittivity of air and $V(r)$ is the applied voltage. The membrane deflection $s(r)$ is governed by the membrane equation

$$T\nabla^2 s + p = \rho \frac{\partial^2 s}{\partial t^2}, \quad (2)$$

where $T = \sigma h$ is the in-plane tension of the membrane with thickness h and stress σ , and ρ is the area mass density. For static solutions the acceleration term is zero. When the same voltage is applied to all electrodes and the deflection is small, the membrane shape $s(r)$ is parabolic with maximum deflection s_0 given by

$$s_0 = \frac{\epsilon_0 V^2 r_0^2}{8g^2 \sigma h}, \quad (3)$$

where r_0 is the mirror radius. For large deflection, the shape deviates from a parabola, and must be calculated from a numerical solution of the membrane equation.

This MOEMS mirror is intended for focus control and spherical aberration correction, so the membrane and actuating electrodes have circular symmetry. If the deflected shape $s(r)$ is fit to a polynomial, only even powers of r are used. The quadratic term is dominant and determines the optical power. Higher order terms describe spherical aberration that will be imparted to the reflected beam. These terms may be undesirable, as when reflecting a collimated beam that is unaberrated, or they may be intentional and used to compensate for aberration already present on the incident beam. Figure 1(b) shows the use of independent voltages to achieve the resultant shape of the membrane to control aberration.

3 Fabrication Process

The fabrication process for the MOEMS deformable mirror is illustrated in Fig. 2. The SU-8 focus control mirror is fabricated using two 100-oriented silicon wafers with an adhesive wafer bonding process. One wafer called the spacer wafer supports control electrodes and uses a thick SU-8 film to create the cavity beneath the membrane. The spacer wafer is oxidized and three concentric aluminum electrodes are patterned on the polished side for electrostatic actuation. Then the wafer is coated with 22 μm SU-8 2025 (Microchem, Inc.)

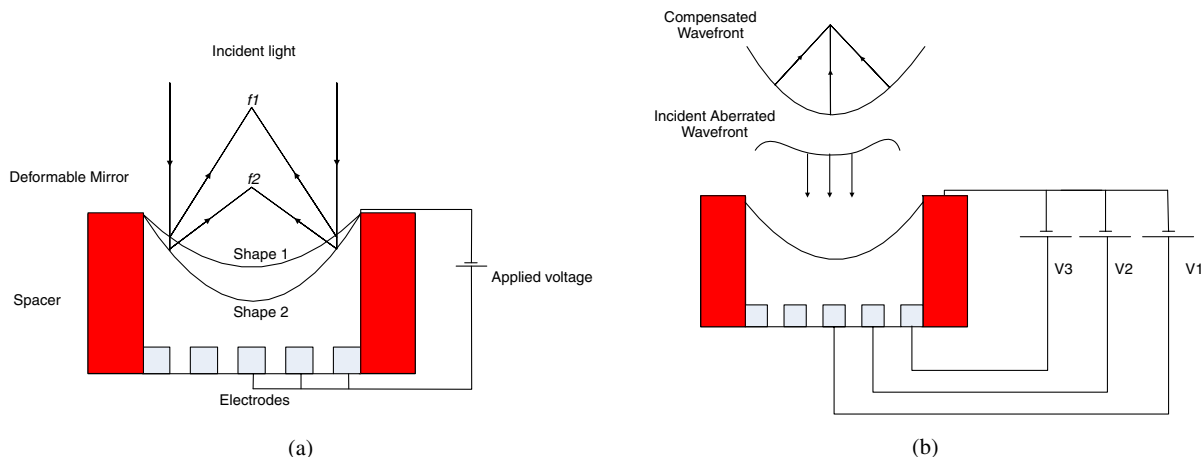


Fig. 1 Principle of operation for deformable membrane mirror (a) focus control: shape 1 with smaller deflection results in larger focal length (f_1), shape 2 with larger deflection results in smaller focal length (f_2) and (b) spherical aberration correction: the shaped mirror cancels the spherical aberration error on the wavefront and focuses all rays at the focal point.

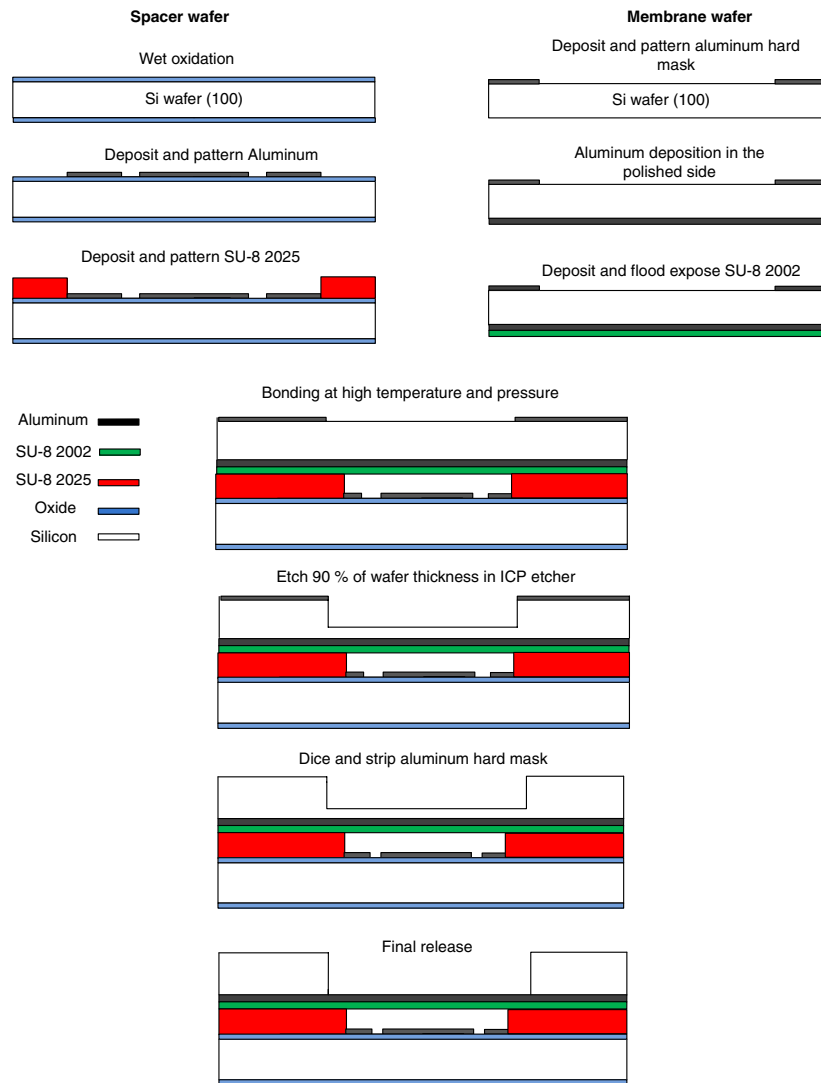


Fig. 2 Fabrication process for deformable membrane mirrors.

using a spin coating procedure. The thick SU-8 is patterned to form the spacer and create the cavity and air channels. The air channels allow airflow into and out of cavity. The deformable mirrors are created on the second wafer called the membrane wafer. First, 100 nm aluminum and then 2 μm SU-8 2002 are deposited on the polished side of the silicon wafer to establish a smooth metalized polymer film. Aluminum is also deposited and patterned on the back side of the membrane wafer as a hard mask to define etch windows for subsequent through-wafer etch. The SU-8 membrane layer is prebaked on a hotplate at 65°C for 90 s, then the temperature is ramped at 6.7°C/s up to 95°C and maintained at 95°C for 90 s, then the wafer is removed to a steel cleanroom table to cool. The wafer is flood exposed to ultraviolet (UV) light with intensity 19.5 mW/cm² for 5 s to crosslink the SU-8 layer. A post exposure bake is carried out with temperature profile identical to the preexposure soft bake process. Since both wafers are coated with an SU-8 layer, they can be bonded under high pressure and temperature.

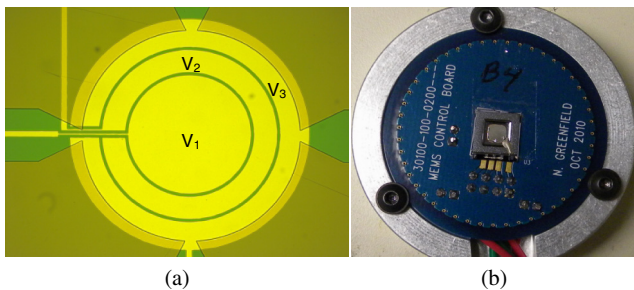
The wafers are aligned using a digital camera and then bonded at a temperature of 145°C for 90 min. The wafers are squeezed between two aluminum plates using a torque wrench and standard 1/4-20 screw. The torque wrench applies

5 N-m of torque to the screw resulting a pressure of approximately 300 kPa to the wafers. After bonding, the mirrors are released by etching through the membrane wafer using a DRIE process. DRIE is performed in an inductively coupled plasma (ICP) etcher using sulfur hexafluoride (SF₆) and oxygen (O₂) as process gases.²² The parameters for dry etching are shown in Table 1.

The etching process is performed in two steps. First 90% of the silicon (450 μm) on the membrane wafer is etched in the ICP etcher. After stripping the aluminum hard mask and dicing the bonded wafer, final etching creates the free-standing membrane mirrors. Because the aluminum hard mask is sputtered during the etch, it can leave particles on the mirrors even though the selectivity between aluminum and silicon is very high. By etching in two steps, stripping the aluminum mask before the final 50 μm are etched, the mirrors stay clean and shiny. Also, the fragile membranes can be damaged during dicing due to water pressure and silicon particles. The 50 μm layer of silicon on the membranes protects the mirrors during the dicing step. Finally, individual devices are mounted and wire bonded to a circuit board. Figure 3 shows one device on a completed spacer wafer and the final mounted device.

Table 1 DRIE parameters for silicon etching.

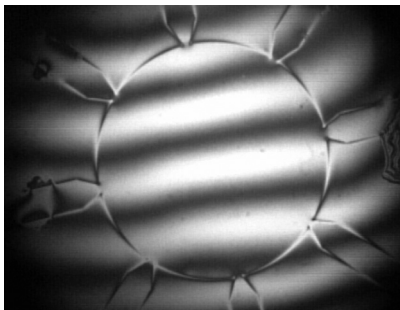
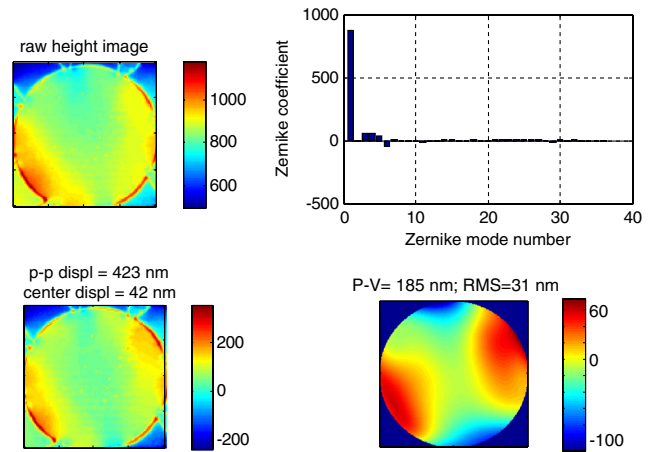
Parameters	Value
SF ₆	82 sccm
O ₂	18 sccm
ICP power	1500 W
RIE power	5 W
Main chamber pressure	15 mTorr
Stage temperature	25°C
Hard mask	200 nm aluminum
Si (100) etch rate	7 μm/min

**Fig. 3** (a) A single device with actuating electrodes and 22 μm patterned SU-8 layer on spacer wafer and (b) the final device with overall chip size 10 × 9 mm² glued and wire bonded to a circuit board.

4 Mirror Optical Properties

The optical properties such as initial flatness and aberration are very important for deformable membrane mirrors. Since the membrane mirror is created on the polished side of the silicon wafer, the initial flatness is superior. Moreover, wafer bonding results in higher uniformity of stress on the membrane relative to devices fabricated by bonding individual die. Figure 4 shows the excellent flatness for a 2-mm diameter mirror at rest when imaged using an optical interferometer.

Figure 5 shows a surface profile, obtained using a phase-shift interferometer, for a 2-mm diameter membrane with no applied voltage, showing its baseline surface height

**Fig. 4** The initial flatness of 2-mm diameter membrane mirror at rest, imaged using an optical interferometer with $\lambda = 830$ nm.**Fig. 5** A 2-mm diameter membrane with no applied voltage; the raw height information (upper left), coefficients for the best fit Zernike polynomials (upper right), the data with tilt and offset removed (lower left) and the residual aberration reconstructed from the Zernike spectrum with tip, tilt, offset and parabolic curvature removed (lower right). Scale bars indicate displacement in nm.

variation. The figure shows raw height information (upper left) and coefficients for the best fit Zernike polynomials (upper right),²³ an image with tip, tilt and offset removed (lower left) and residual aberration reconstructed from the Zernike spectrum after subtracting tilt, offset and parabolic curvature (lower right). Table 2 specifies the Zernike

Table 2 Zernike basis set (through mode 15) used to fit the measured surface height profile.

Term #	Polynomial	Aberration type
1	1	Piston
2	$r \cos(\theta)$	Tilt about y-axis
3	$r \sin(\theta)$	Tilt about x-axis
4	$r^2 \cos(2\theta)$	Astigmatism
5	$2r^2 - 1$	Defocus
6	$r^2 \sin(2\theta)$	Astigmatism
7	$r^3 \cos(3\theta)$	Trefoil
8	$(3r^3 - 2r) \cos(\theta)$	Coma
9	$(3r^3 - 2r) \sin(\theta)$	Coma
10	$r^3 \sin(3\theta)$	Trefoil
11	$r^4 \cos(4\theta)$	Quadrafoil
12	$(4r^4 - 3r^2) \cos(2\theta)$	2nd Astigmatism
13	$6r^4 - 6r^2 + 1$	Spherical
14	$(4r^4 - 3r^2) \sin(2\theta)$	2nd Astigmatism
15	$r^4 \sin(4\theta)$	Quadrafoil

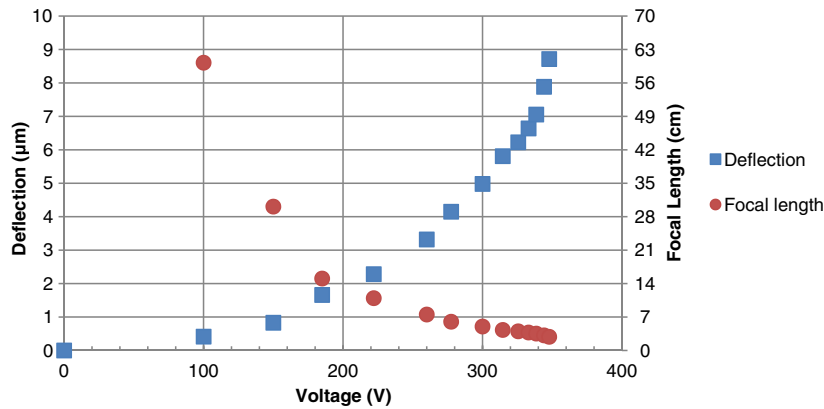


Fig. 6 Center deflection and focal length versus applied voltage for circular mirror 2 mm in diameter, with 22 μm cavity beneath the membrane.

polynomials corresponding to the spectrum. Peak to valley residual aberration is 185 nm for this device, with root mean square (RMS) aberration of 31 nm. This information indicates the residual aberration for a wafer bonded device is less than for a die bonded mirror.¹⁵ Initial surface errors (such as astigmatism) have been decreased by the new fabrication process.

5 Focus Control

The membrane mirrors are deflected with electrostatic force by applying a DC voltage to the electrodes and keeping the membrane at ground potential. Figure 6 shows the center deflection and focal length versus driving voltage for a 2-mm diameter mirror. The focal length of a mirror in air is calculated by $f = r_0^2/4s_0$ where r_0 is membrane radius and s_0 is center deflection. When the mirror is flat the focal length is infinite. When the center deflection is 8.7 μm the focal length is 2.8 cm. In this measurement, the applied voltage is the same for all three electrodes. Displacement to approximately 40% of the air gap is observed without snapdown.

The membrane displacement is measured using an optical phase-shift interferometer. Figure 7 shows an optical interferogram image of the deflected membrane. In this image, each fringe represents a half wavelength displacement while the laser source wavelength is 830 nm. The maximum

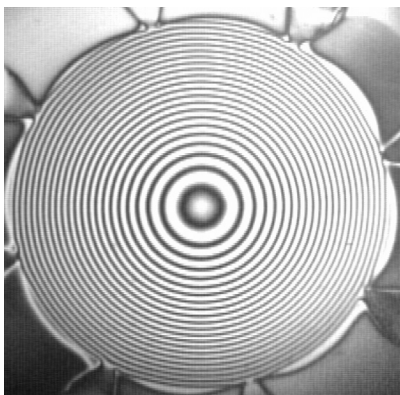


Fig. 7 Optical interferogram image ($\lambda = 830$ nm) of 2 mm mirror at DC voltage of 348 V.

deflection achieved for a circle with 2-mm diameter at 348 V is 8.7 μm . The pull-in voltage is measured as 360 V, when the membrane is reversibly stuck down to the electrodes. The membrane deflection depends on the thin film intrinsic stress, with a film with lower stress deflecting more at the same electrostatic force. The intrinsic stress on the membrane can be calculated using Eq. (3) by knowing the film deflection and the mirror geometry. These data indicate an intrinsic stress for the SU-8 film of approximately 20 MPa.

The mirror deflection changes the focal distance, and consequently the defocus term appears in the Zernike spectrum in Fig. 8. When the center of the membrane is deflected 4.9 μm (300 V applied to each electrode), the dominant Zernike coefficient is defocus corresponding to mode number 5 ($2r^2 - 1$ in our basis set, where r is the normalized pupil radius). The dominant surface errors (excluding tip, tilt and piston) at this voltage are astigmatism (mode numbers 6 and 12) and spherical aberration (mode number 13). Residual aberration is still low at only 98 nm RMS. Figure 8 shows the optical parameters with this uniform applied voltage of 300 V. Subplots are the same as for Fig. 5.

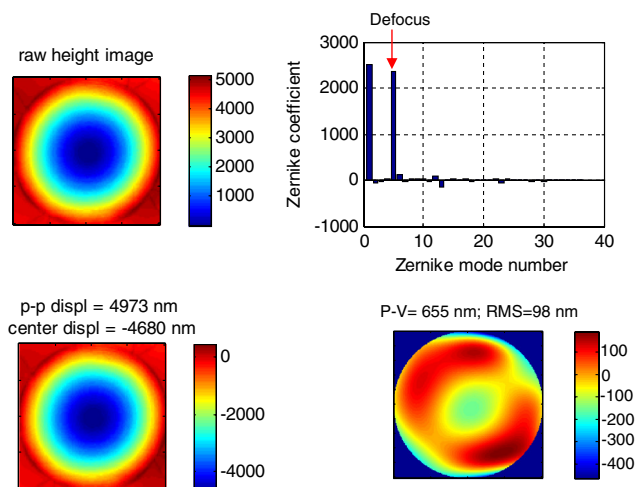


Fig. 8 Optical parameters of a 2-mm diameter mirror for uniform applied voltage of 300 V. Subplots are the same as in Fig. 5.

6 Spherical Aberration Correction

The deformable MOEMS mirror is also able to introduce spherical aberration by shaping the membrane. With uniform pressure, the membrane shape is parabolic and the spherical aberration is zero. At larger deflection the electrostatic pressure with a uniform voltage is not uniform but is influenced by the decreasing air gap as the membrane deflects. Therefore the membrane shape is not exactly parabolic and spherical aberration is introduced to the mirror profile. The mirror shape is adjustable by applying different voltages to the electrodes in order to cancel the optical aberrations. Figure 9 shows the Zernike spectrum for different voltages applied to the electrodes. When 220 V is applied to all electrodes the maximum deflection is $2.3 \mu\text{m}$ (less than 11% of the air gap) and the mirror shape is nearly parabolic and the spherical aberration, mode number 13, has a coefficient of 35 nm in the Zernike spectrum [Fig. 9(a)]. Setting the middle electrode at 320 V and the two other electrodes at 220 V results in 125 nm spherical aberration coefficient (mode 13) in the mirror surface profile [Fig. 9(b)]. The mirror with such a voltage pattern is able to correct 250 nm of negative wavefront spherical aberration (the wavefront modification is twice the surface height variation). Setting the center electrode at 320 V and the outer two electrodes at 220 V, mode number 13 is again the dominant aberration coefficient, but it is negative now as shown in Fig. 9(c). The overall dominant term is still defocus, mode 5. The Zernike coefficient for mode 13 is more than 350 nm. This result indicates the device can compensate positive spherical aberration of the wavefront of as much as 700 nm. Expressed in terms of peak-to-peak amplitude of balanced spherical aberration, the full adjustment range (positive and negative) of the mirror is $1.5 \times (250 + 700) = 1.4 \mu\text{m}$, where the factor of 1.5 is derived from the peak-to-peak amplitude of mode 13.

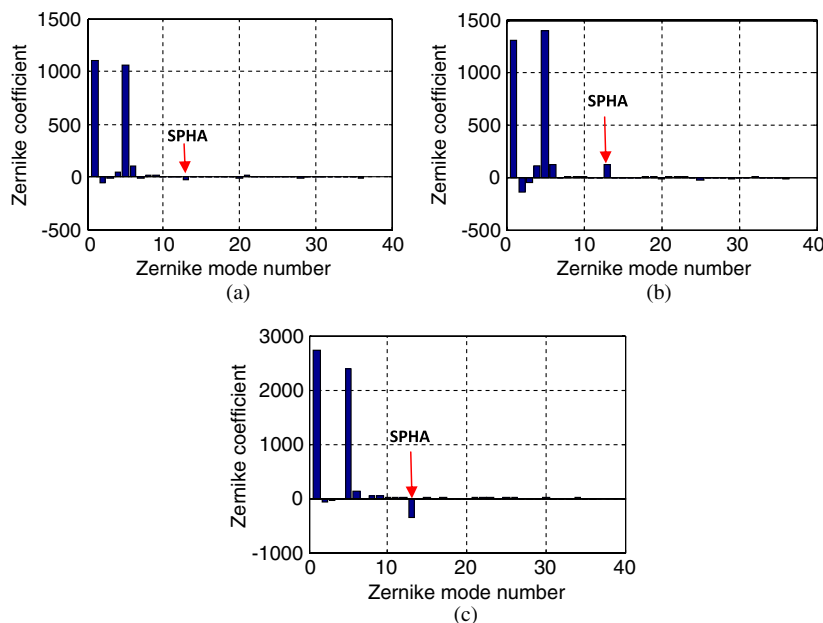


Fig. 9 Zernike spectrum of a 2-mm diameter mirror (a) small spherical aberration (35 nm); uniform voltage 220 V on the all three electrodes ($V_1 = V_2 = V_3 = 220 \text{ V}$), (b) positive spherical aberration correction; the middle electrode voltage is 320 V and the two other electrodes are kept at 220 V ($V_1 = 220, V_2 = 320, V_3 = 220 \text{ V}$), and (c) negative spherical aberration (SPHA) correction; the inner electrode voltage is 320 V, and the outer electrodes are 220 V ($V_1 = 320, V_2 = 220, V_3 = 220 \text{ V}$)

Figure 10 shows surface height maps of the residual aberrations for negative and positive spherical aberration on the membrane, corresponding to the Zernike spectra of Fig. 9(b) and 9(c). Astigmatism (modes 4 and 6) superimposed with the positive spherical aberration is obvious in Fig. 10(a). Peak-valley of the residual aberration is 430 nm for this case. For negative spherical aberration the Peak-valley is 722 nm.

7 Focus Control in Scanning Confocal Microscopy

The MOEMS deformable mirror is used in a confocal scanning laser microscope to control the focus and capture *in situ* images of plant tissue. Figure 11 shows the schematic of the confocal microscope using the variable focus control MOEMS mirror. A 70 mW near infra red (IR) laser source is used to illuminate the sample. An 830 nm wavelength laser beam passes through the half wave plate to control the polarization state of the light. A beam splitter is used to separate the incident laser beam and the reflected signal from the sample. The incident beam reaches the tilted ($\sim 3^\circ$) 2-mm diameter MOEMS focus control mirror and the reflected beam is guided to the scanning MOEMS mirror (Microvision, Inc.) through the mirror M1 and lenses L1 and L2. The focus control mirror adjusts the imaging depth (z-direction) and the scanning MOEMS mirror scans the sample surface (x-y plane). The telescope lenses L1-L4 are used to adjust the beam size and simultaneously form an image of the focus control mirror and scan mirror at the back focal plane of the objective lens. The quarter wave plate converts linearly polarized light to circular for the forward path, while converting the reflected circular polarization back to linear, rotated 90 deg with respect to the illumination beam. The reflected light carrying the tissue image information is separated at the polarizing beam splitter. The coupling lens focuses the beam onto the core of a single mode optical fiber. The optical fiber is connected to an avalanche photodiode (APD) in order to convert the optical signals to

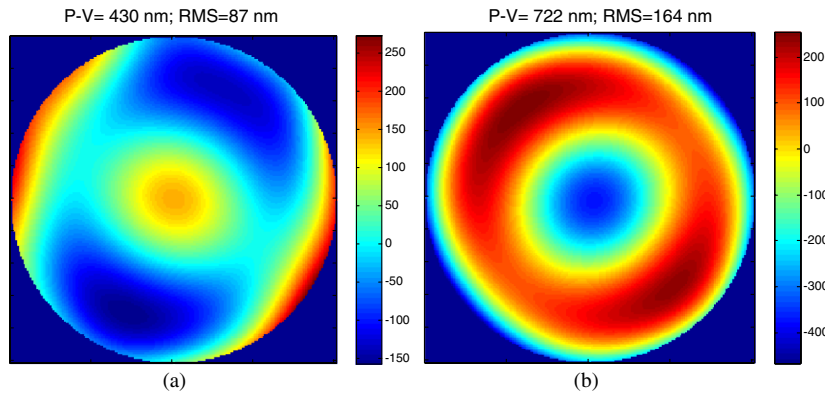


Fig. 10 Residual aberration profile on the membrane (a) positive spherical aberration ($V_1 = 220$, $V_2 = 320$, $V_3 = 220$ V) and (b) negative spherical aberration ($V_1 = 320$, $V_2 = 220$, $V_3 = 220$ V).

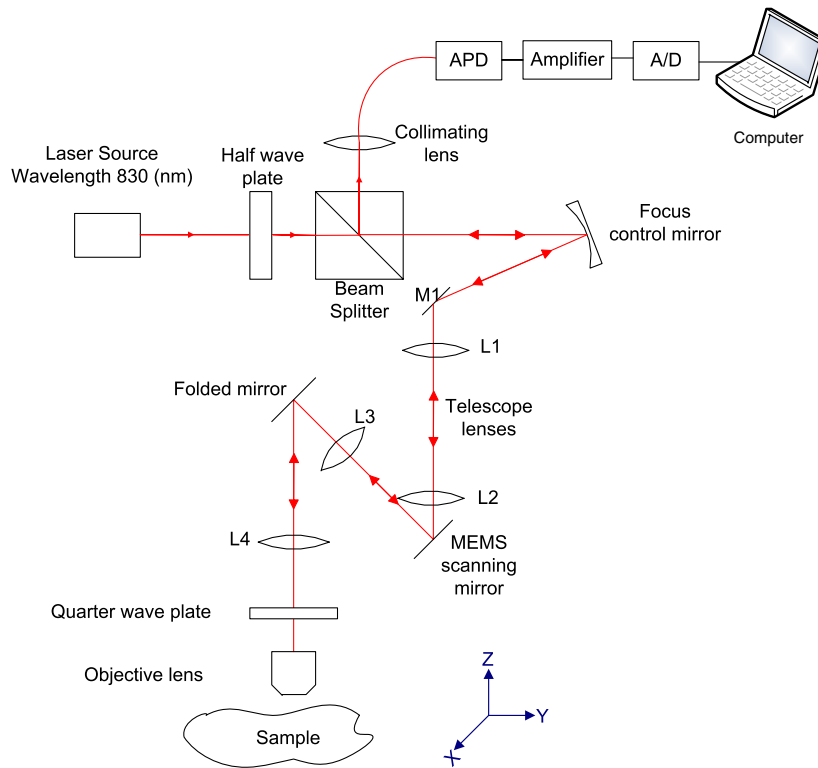


Fig. 11 Variable focus control confocal microscopy.

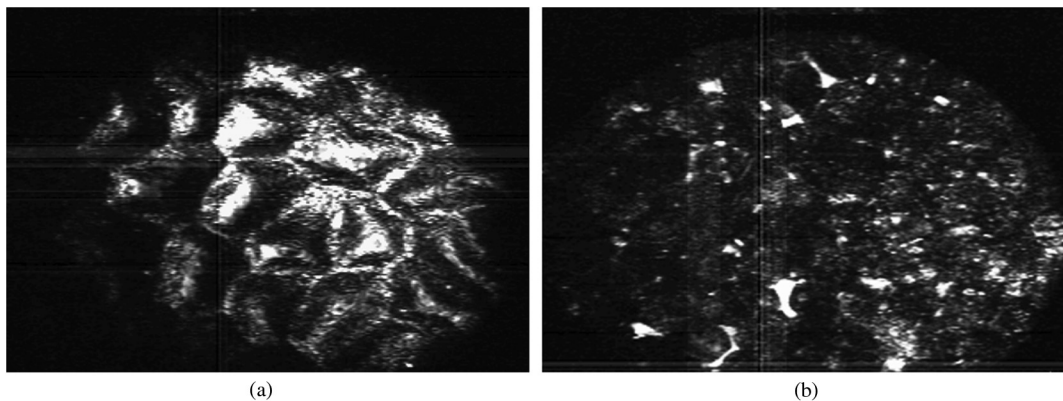


Fig. 12 Optical microscopy of arrowhead syngonium leaf tissue (a) 330 V on the focus control mirror: the focus is on the surface of the leaf convex cells and (b) 270 V on the focus control mirror: the focus is beneath the upper epidermis layer.

electrical signals. Then the electrical signals are amplified and digitized to form the images on the computer. The objective lens numerical aperture (NA) is 0.9.

Living arrowhead syngonium leaf tissue has been imaged using this microscope. The sample is fixed with respect to the objective lens and the voltage on the focus control mirror adjusts the imaging depth. Figure 12(a) shows the leaf convex cells in the upper epidermis layer when the voltage on the focus control mirror is 330 V. Then the voltage is set to 270 V and the focus is changed to the mesophyll layer as shown in Fig. 12(b). The focus range corresponding to 7 μm membrane deflection is 42 μm in the leaf tissue.

8 Conclusion

An improved process to fabricate SU-8 deformable mirrors capable of focus control and limited spherical aberration correction has been described in this work. Initially flat mirrors 2 mm in diameter were demonstrated. A relatively low temperature wafer bonding process that replaces a hardbake step resulted in estimated residual stress in the SU-8 membrane of 20 MPa. The 2-mm diameter circular mirror achieved 8.7 μm center deflection at uniform applied voltage of 348 V, with a 22 μm air gap, limited by snapdown. Previously we have demonstrated actuation using more than 400 V with these materials without breakdown, indicating that a larger air gap and greater deflection is possible by using a thicker spacer layer.

Importantly, the initial surface quality is improved with the wafer-scale bonding, compared to the prior die bonding approach.¹⁵ The residual aberration on a 2 mm diameter circular membrane is reduced to 31 nm RMS at rest, increasing to 98 nm RMS for 4.9 μm center deflection. This surface error is acceptable for applications such as biomedical imaging using near infrared wavelengths. Furthermore, this device can minimize spherical aberration originating elsewhere in the system by shaping the mirror through applying different voltages to the control electrodes. We hope to use this capability to maintain or improve image quality during focus adjustment in our future work.

We also demonstrated here for the first time MOEMS focus control while imaging living plant tissue. We note that the range of focus adjustment at high NA in an aqueous medium (like living tissue) is still limited (42 μm in our experiment for 7 μm membrane deflection, using NA = 0.9), demanding mirrors in the future with greater stroke. Because the focus adjustment range is proportional to the stroke, we need to increase our mirror deflection by a factor of four to five to achieve useful full-range focus adjustment in scattering tissues like skin where confocal microscopy is capable of penetration to a depth of 150 to 200 μm . We are optimistic that this technology will be capable of these larger strokes while maintaining low optical aberration to achieve diffraction limited performance.

Acknowledgments

This project was supported by the National Science Foundation under Award No. 0754608 and 0956910, and the Montana Board of Research and Commercialization Technology Grant No. 11-24. The device was fabricated at the Montana Microfabrication Facility at Montana State University.

References

1. B. Berge and J. Peseux, "Variable focal lens controlled by an external voltage: an application of electrowetting," *The Eur. Phys. J. E: Soft Matter Biol. Phys.* **3**(2), 159–163 (2000).
2. S. Kuiper and B. H. W. Hendriks, "Variable-focus liquid lens for miniature cameras," *Appl. Phys. Lett.* **85**(7), 1128–1130 (2004).
3. H. Ren and S.-T. Wu, "Variable focus liquid lens," *Opt. Express* **15**(10), 5931–5936 (2007).
4. H. Ren, S. Xu, and S.-T. Wu, "Deformable liquid droplets for optical beam control," *Opt. Express* **18**(11), 11904–11910 (2010).
5. S. Xu et al., "A novel adaptive mechanical-wetting lens for visible and near infrared imaging," *Opt. Express* **18**(12), 12430–12435 (2010).
6. D. W. Lee and Y.-H. Chu, "A 4 bit digital liquid lens for variable focal length," *J. Micromech. Microeng.* **20**, 035029 (2010).
7. F. Schneider, C. Müller, and U. Wallrabe, "A low cost adaptive silicon membrane lens," *J. Opt. A: Pure Appl. Opt.* **10**, 044002 (2008).
8. K.-H. Jeong et al., "Tunable microdoublet lens array," *Opt. Express* **12**(11), 2494–2500 (2004).
9. D. Mader, A. Seifert, and H. Zappe, "Fabrication of aberration-corrected tunable micro-lenses," in *2008 IEEE/LEOS International Conference on Optical MEMs and Nanophotonics*, Freiburg, pp. 60–61 (2008).
10. P. M. Moran et al., "Fluidic lenses with variable focal length," *Appl. Phys. Lett.* **88**(4), 041120 (2006).
11. H. Oku and M. Ishikawa, "High-speed liquid lens with 2 ms response and 80.3 nm root-mean-square wavefront error," *Appl. Phys. Lett.* **94**(22), 221108 (2009).
12. H. Ren et al., "Tunable-focus liquid lens controlled using a servo motor," *Opt. Express* **14**(18), 8031–8036 (2006).
13. A. Werber and H. Zappe, "Tunable pneumatic microoptics," *J. Microelectromech. Syst.* **17**(5), 1218–1227 (2008).
14. C. Friese and H. Zappe, "Deformable polymer adaptive optical mirrors," *J. Microelectromech. Syst.* **17**(1), 11–19 (2008).
15. M. J. Moghimi et al., "MOEMS deformable mirror for focus control in vital microscopy," *J. Micro/Nanolith. MEMS MOEMS* **10**(2), 023005 (2011).
16. G. Vdovin and P. M. Sarro, "Flexible mirror micromachined in silicon," *Appl. Opt.* **34**(16), 2968–2997 (1995).
17. P. A. Himmer, D. L. Dickensheets, and R. A. Friholm, "Micromachined silicon nitride deformable mirrors for focus control," *Opt. Lett.* **26**(16), 1280–1282 (2001).
18. J. Wang et al., "Miniature optical autofocus camera by micromachined fluoreopolymer deformable mirror," *Opt. Express* **17**(8), 6268–6274 (2009).
19. P.-Y. Lin, H.-T. Hsieh, and G.-D. John Su, "Design and fabrication of a large-stroke MEMS deformable mirror for wavefront control," *J. Opt.* **13**(5), 055404 (2011).
20. S. J. Lukes and D. L. Dickensheets, "SU-8 focus control mirrors released by XeF₂ dry etch," *Proc. SPIE* **7930**, 793006 (2011).
21. K. W. Oliver et al., "Stress engineering for free-standing SU-8 2002 thin film devices," *Proc. SPIE* **8248**, 82480H (2012).
22. B. A. Ganji and B. Y. Majlis, "Deep trenches in silicon structure using DRIE method with aluminum as an etching mask," in *IEEE International Conf. on Semiconductor Electronics, 2006 (ICSE '06)*, Kula Lumpur, Malaysia, pp. 41–47 (2006).
23. P. Fricker, "Zernike polynomials," MATLAB Central File Exchange, Updated 11 Mar 2008, <http://www.mathworks.com/matlabcentral/fileexchange/7687-zernike-polynomials> (2010).



Mohammad J. Moghimi received his BS degree in electrical engineering from K. N. Toosi University of Technology, Tehran, Iran, in 2005 and his MS degree in electrical engineering from Amirkabir University of Technology, Tehran, Iran, in 2008. He is currently a PhD student developing new MEMS devices and fabrication techniques especially for micro-optical components at Montana State University, Bozeman, Montana.



Chris R. Wilson received his BS degree in mechanical engineering from Montana State University in 2005 and is currently pursuing a masters degree in systems engineering from Penn State. He is currently a mechanical engineer at Bridger Photonics, Inc., developing MEMS deformable mirrors as well as lasers for the metrology and medical fields.



David L. Dickensheets received his PhD in electrical engineering from Stanford University in 1997. From 1996 to 1997 he was a research associate in the Edward L. Ginzton Laboratory at Stanford University. In 1997, he joined the faculty at Montana State University in Bozeman, where he is currently a professor of electrical engineering. His research interests include optical imaging and spectroscopy of tissues, and the application of microfabrication technologies to develop

miniature optical instruments for biomedical and industrial imaging applications, telecommunications, and planetary exploration.